



Energy and Exergy Analyses of Stirling Engine using CFD Approach

Sherihan El-Ghafour^{1,*}, Nady Mikhael¹, Mohamed El-Ghandour¹

¹ Mechanical Power Engineering Department, Faculty of Engineering, Port-Said University, Port-Said, Egypt

ARTICLE INFO

Article history:

Received 8 May 2020

Received in revised form 24 July 2020

Accepted 25 July 2020

Available online 4 November 2020

ABSTRACT

A comprehensive characterization of the GPU-3 Stirling engine losses with the aid of the CFD approach is presented. Firstly, a detailed description of the losses-related phenomena along with the method of calculating each type of loss are addressed. Secondly, an energy analysis of the engine is carried out in order to specify the impact of each type of losses on the performance. Finally, the design effectiveness of each component of the engine is investigated using an exergy analysis. The results reveal that the hysteresis loss occurs mainly within the working spaces due to the flow jetting during the first part of the expansion strokes. Additionally, the pressure difference between the working spaces is the main driver for the flow leakage through the appendix gap. The exposure of the displacer top wall to the jet of hot gas flowing into the expansion space during expansion stroke essentially increases the shuttle heat loss. A new definition for the regenerator effectiveness is presented to assess the quality of the heat storage and recovery processes. The energy analysis shows that regenerator thermal loss and pumping power represent the largest part of the engine losses by about 9.2% and 7.5% of the heat input, respectively. The exergy losses within regenerator and cold space are the highest values among the components, consequently, they need to be redesigned

Keywords:

Stirling engine; Losses; Energy and exergy analyses; CFD simulation

1. Introduction

Computational Fluid Dynamics (CFD) approach provides an essential contribution to the simulation of Stirling engine especially with the increasing need for high-accuracy models. Indeed, the CFD models have recently achieved high accurate predictions of the Stirling engine performance [1, 2]. This is, besides, the successfulness in the depiction and explanation of the highly transient phenomena related to the fluid dynamics and heat transfer within the engine [1, 3]. Furthermore, this technique has effectively dealt with the complicated geometry of this engine and the consequent

* Corresponding author.

E-mail address: s.a.ghafour@eng.psu.edu.eg

<https://doi.org/10.37934/arfmts.77.1.100123>

three-dimensional effects [4, 5]. All these aspects have been considered as obstacles facing the conventional zero- and one-dimensional numerical techniques [1].

The losses of the Stirling engine have always been a topic of substantial interest to researchers concerned with the performance analysis. Nevertheless, the accurate estimation of these losses is still one of the most common problems of the engine modeling due to the difficulty of understanding and prediction of the irreversibilities causing them. There are different categories upon which these losses can be classified [6-8]. In general, the losses of Stirling engine can be mainly classified as thermal, flow and mechanical losses. The thermal losses include hysteresis loss, regenerator heat loss, shuttle heat transfer by the displacer, enthalpy pumping losses through the appendix gap as well as heat conduction loss through the walls of the regenerator and the cylinder. Whereas the pumping loss, the power loss due to piston finite speed and the leakage from the piston seal are classified as the flow ones. In the following subsections, an identification of each type of loss along with the previous attempts of its estimation will be presented.

1.1 Hysteresis Loss

The cyclic heat transfer rate, heat pumping, through the walls of the working spaces is usually referred to as “hysteresis loss”. This occurs due to the heat interaction between the working gas and the walls of these spaces. Tew [9] pointed out that regions with small surface-to-volume ratio, such as working spaces and manifolds, are generally responsible for the hysteresis loss. However, the several irreversible processes that occur within the working spaces are the main reason for this type of loss. These processes include the gas spring, the jetting and ejecting flow which usually accompanying by eddy motions and the mixing of gases at different temperatures.

For a long time, almost all research has been focused on the gas spring as the only source of hysteresis loss. The compressibility of the gas enclosed within a cylinder-piston arrangement is used to provide a force when subjected to a displacement work such that provided by the mechanical spring [10]. When the gas spring is first compressed and then allowed to expand back to the initial state, a certain amount of work is dissipated [11]. Various analytical and empirical equations have been developed to predict hysteresis losses in the gas spring [12-14]. Though, the analytical equation derived by Urieli and Berchowitz [14] is particularly considered as the most applied one in Stirling engine analyses. However, the discrepancy between the experimental data and the theoretical predictions motivates the researchers to include the other irreversible effects in the derived equations. Correction factors were initially applied to these equations to enhance the estimation of this loss [15]. Afterwards, Kornhauser [11] derived an empirical correlation for the hysteresis loss when the cylinder is connected with a heat exchanger. However, this correlation is not adequate for the loss prediction in the whole operating conditions that exist in the Stirling engine. Recently, Willich *et al.*, [16] presented an axisymmetric CFD model of the gas spring. They observed a significant increase in hysteresis loss due to the presence of the eddy motions such as generated from the flow through valves or any source of secondary flow.

In this context, it is worth mentioning that there is a contradiction in published literature concerning the influence of the hysteresis loss on the Stirling engine performance. Urieli and Berchowitz [14] stated that the crank-type Stirling engines usually have small hysteresis loss, while Timoumi *et al.*, [17] and Sullivan [18] confirmed that the inaccuracy in the estimation of the hysteresis loss has a significant impact on the performance prediction error regardless the Stirling engine type.

1.2 Regenerator Thermal Loss

Generally, the gas flow within the regenerator goes through two periods, namely, hot and cold blows. The regenerator matrix is considered as a thermal storage element during the hot blow period. In this period, the energy of the hot flow coming from the heater is absorbed in the regenerator matrix. Subsequently, it gives up this energy to the cold gas flowing from the cooler during the cold blow period [1]. In practice, it is impossible to have heat storage or recovery flawlessly.

Typically, the quality of regeneration process is evaluated by the regenerator effectiveness. Urieli and Berchowitz [14] defined the effectiveness as “the amount of heat transferred from the matrix to gas during a single blow through the regenerator to the equivalent amount of heat transferred in the regenerator of the ideal adiabatic model”, while Timoumi *et al.*, [17] proposed another definition based on enthalpy changes as “the actual enthalpy change of the gas during a single blow to the maximum theoretical enthalpy change of the gas in the regenerator”. The definition of Timoumi is mostly used. However, it depends mainly on the assumption of a linear distribution of the gas temperature inside the regenerator. The weakness of this assumption is later confirmed in other studies [1, 19, 20]. The regenerator thermal loss is considered one of the most major losses that affect the performance of the Stirling engine [9, 10, 14, 17, 21].

1.3 Shuttle Heat Transfer and Enthalpy Pumping Losses

In β - and γ -configurations of the Stirling engine, the reciprocating motion of the displacer alternatively shuttles the working fluid from the hot to the cold space. This reciprocating motion is accompanied by two different types of thermal losses; shuttle heat transfer and enthalpy pumping losses. Besides the conduction loss resulting from the axial temperature gradient along the walls of the displacer and the cylinder, the reciprocating motion of displacer causes extra heat transfer from the hot to the cold space. This motional heat transfer is so-called shuttle heat transfer [22]. The basic principle of the shuttle heat transfer is illustrated in Figure 1. When the displacer reaches the hot end of its stroke, the displacer walls receive heat from the cylinder walls. Contrarily, the heat is transferred from the displacer walls to the cylinder walls during the movement of the displacer towards the cold end of its stroke. As the cycle proceeds, the displacer repeatedly receives heat from the expansion space and rejects heat to the compression space. This creates a cyclic net enthalpy flow rate from the expansion to the compression space – that is the shuttle heat transfer [23].

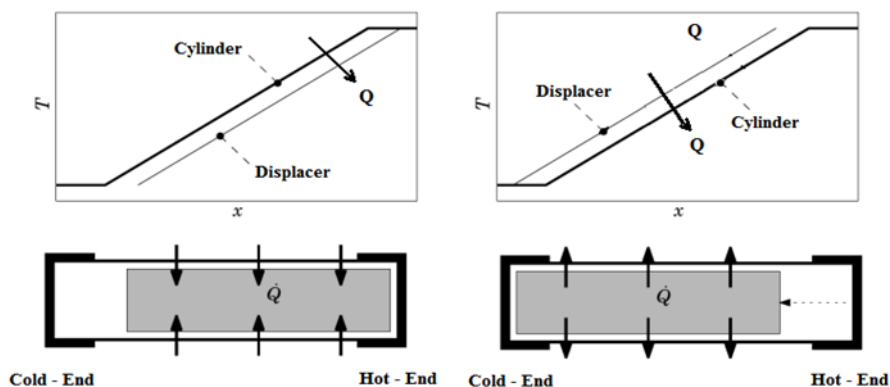


Fig. 1. Schematic diagram of basic principles of shuttle heat transfer [24]

In addition to the energy carried by the reciprocating displacer, the presence of the appendix gap causes other type of loss. The enthalpy pumping loss, which is the flow leakage through this gap that yields a cyclic net enthalpy flow rate in the presence of axial temperature gradient [23]. The enthalpy pumping is one of the most complicated losses in Stirling engine. The complex fluid flow and heat transfer phenomena taking place in the appendix gap result from a combination of pressure fluctuations and displacer motion in the presence of axial temperature gradient [24]. Moreover, the overlapping between this loss and the shuttle heat transfer loss causes a difficulty of dealing with each loss separately.

Several analytical and empirical expressions were proposed to estimate the shuttle heat transfer and the enthalpy pumping losses. Rios [25] firstly derived a simple expression for calculating only the shuttle loss. This expression was based on the assumptions of infinite heat capacity for the cylinder and displacer walls as well as a sinusoidal motion for the displacer. Later, Urieli and Berchowitz [14] and Martini [26] used Rios's formula in their analysis. On the other hand, Urieli and Berchowitz [14] modelled the flow in the appendix gap as a steady Couette flow and derived a simple formula for the leakage mass flow through the appendix gap. This formula has been used in Stirling engine analysis till now. These models had been followed by several attempts to obtain more accurate results [22-24, 27]. However, all these studies used simple geometries to derive closed formulas for the shuttle and enthalpy pumping losses. Recently, Sauer and Kuehl [28] pointed out the importance of coupling the differential equations of the appendix gap to the main differential equations of the whole engine. This can achieve more accurate estimation for these losses compared with the analytical models which are based on partially questionable assumptions and simple geometries.

Interestingly, there is a contradiction in the published literature concerning the influence of the shuttle and enthalpy pumping losses on the Stirling engine performance. Some researchers [29] confirmed on the small influence of these losses on the engine performance and, hence, neglected them in their analysis, while other studies confirmed that it cannot be negligible as it may amount to about 10% of the total heat input [30].

1.4 Heat Conduction Loss through Engine Walls

In general, the temperature gradient along the Stirling engine promotes a heat conduction loss through the walls of the engine. Most of this heat conduction loss appears through the walls of the regenerator which separates the heater and the cooler [31]. Also, the heat conduction from the hot space to the cold space through the cylinder walls is another source of this type of loss [32]. According to Fourier's law, the heat loss by conduction through the walls of the regenerator and the cylinder can be calculated. Here, it should be pointed out that the heat conduction loss through the heater and cooler walls as well as the heat loss due to the gas conductivity can be neglected [17].

1.5 Pumping Loss

In fact, the fluid friction associated with the flow through the heat exchangers and manifolds results in a pressure drop through these components. This consequently has an effect of reducing the power output of the engine, so-called pumping loss [14], [33]. Generally, the pressure drop through the heater, cooler and regenerator is calculated using empirical correlations for the friction coefficient. For a long time, the common practice used the correlations proposed by Kays and London [34] which derived from the steady-state unidirectional flow tests. Since, no correlation has been available for reciprocating flow conditions encountered in Stirling machines until recent years [35].

Recently, several attempts [35], [20] to develop new correlations for friction coefficient through the heater, cooler and regenerator under oscillating flow conditions have been published.

All research emphasizes on the significant impact of pumping loss on the engine performance. According to Ibrahim and Tew [36], the pressure drop losses may represent about 11% of the inefficiency of the Stirling engine and 70 – 90 % of which is attributed to the pressure drop in the regenerator [37]. As well, Simon and Seume [38] referred to that about 35% of the heater and cooler pressure drops occurred at the pipe entrance and exit in the engine.

1.6 Power Loss Due to Piston Finite Speed

During the compression and expansion processes, the actual pressure over the piston face usually differs from the bulk gas pressure in the cylinder according to the flow direction [39]. This pressure loss is due to the piston finite speed. In fact, pressure waves that are generated due to the movement of piston cause this difference [40]. Therefore, the actual power generated by the expansion process is reduced and the actual power consumed in the compression process is increased. As a result, the net power generated by the engine is less than the corresponding power predicted by the classical thermodynamic analysis [41].

Limited number of researchers [39-42] took this type of loss into consideration. They used a simple formula to calculate this pressure loss and combined it with the total pressure drop produced within the heat exchangers.

1.7 Leakage Loss from Piston Seal

In reciprocating machines, the presence of sealing is usually associated with leakage loss. This loss generally occurs between the working spaces and the buffer spaces through the power piston-cylinder gap. The quantity of the mass leakage depends on the size and the power scale of the engine [42]. Different empirical [32] and analytical [14], [43] correlations are used to calculate this loss.

2. Current Contribution

From the above survey, one can observe that the losses estimation were mainly adopted by decoupled and simplified closed-form correlations with several assumptions. This occurred without providing clear relations between the thermodynamics irreversibilities and the physical phenomena that cause them. Also, the researches have differed in the impact of each type of losses on the performance of the Stirling engine. Accordingly, the present study aims at presenting a comprehensive characterization of the physical phenomena causing the losses with the aid of the CFD approach. Then, a detailed energy analysis of the Stirling engine is performed. An exergy analysis of the engine is also conducted in order to accurately assess its performance. The exergy analysis is generally used not only to gauge the potential but also to identify opportunities for improvement in the system performance [44]. The investigation is conducted on a β -type Stirling engine, namely Ground Power Unit-3 (GPU-3). The design specifications of the GPU-3 engine have been documented by El-Ghafour *et al.*, [1, 45]. The detailed three-dimensional CFD simulation and analysis of the GPU-3 engine are performed using a commercial software, ANSYS FLUENT (v14.5).

3. Governing Equations

In the present study, the flow is oscillatory, compressible and Newtonian. Hence, Unsteady Reynolds-Averaged Navier-Stokes (URANS) equations, besides the equation of state, are used to predict the thermal and the fluid flow fields in this model. Here, the realizable k- ϵ model with enhanced wall treatment for the near wall region is employed to estimate the turbulent viscosity. Among the different turbulent and transition models, it was proved to produce the most accurate predictions for the engine performance with a robust convergence for the solution [1]. Additionally, the regenerator is currently modelled using the local thermal non-equilibrium porous media approach. The details of the all applied equations can be found in Ref. [1] and [45].

4. Equations of Energy and Exergy Analyses

The indicated power can be calculated by

$$P_{ind} = \left(\frac{\omega_r}{2\pi}\right) [\phi p_e dV_e + \phi p_c dV_c] \quad (1)$$

The rate of heat transfer over the cycle for any solid boundary is determined as

$$\dot{Q} = \left(\frac{\omega_r}{2\pi}\right) \phi \left(\int_{wall} \dot{q} dA\right) dt \quad (2)$$

The rate of exergy transfer accompanying the heat transfer to or from the system during any process, \dot{E}_q , can be generally written as [44]

$$\dot{E}_q = \left(1 - \frac{T_o}{T_b}\right) \dot{Q} \quad (3)$$

where T_o and T_b denote the temperature of the dead state and of the boundary where heat transfer occurs, respectively. Here, the dead state temperature is assumed as 15°C (288K). On the other hand, the rate of exergy transfer accompanying power, \dot{E}_w , is simply the power [44].

The instantaneous rate of exergy associated with a flowing stream at a specific state, \dot{E}_x , can be computed as

$$\dot{E}_x = (H_x - H_o) - T_o(S_x - S_o) \quad (4)$$

The exergy loss, sometimes called exergy destruction, represents the losses that prevent the system from achieving the maximum efficiency. At the cyclic steady state, the rate of exergy loss, \dot{E}_L , can be calculated from the exergy rate balance for the system as [46]

$$\dot{E}_L = \sum_i \dot{E}_{q_i} + \sum_j \dot{E}_{enter_j} - \sum_k \dot{E}_{w_k} - \sum_l \dot{E}_{exit_l} \quad (5)$$

where \dot{E}_{enter} and \dot{E}_{exit} are the rates of exergy of the flow entering and exiting the system, respectively.

Indeed, there are several methods of exergy analysis that can be conducted on Stirling engine. A method that seems to be more suitable is adopted in the current study. According to this method, a separate exergy balance is applied on each component of the engine. Throughout each balance, the

component is treated as an open system. Hence, the exergy loss within each component can be estimated, as displayed in Eq. (5).

5. Methodology

5.1 Computational Domain

The computational domain at the instance of zero crank angle ($\theta = 0$) is presented in Figure 2. It represents just one-eighth of the engine geometry that consists of heater, cooler, regenerator, displacer and appendix gab in addition to compression and expansion spaces. The wall thickness of these parts is neglected, except that of the displacer. ANSYS Design Modeller is used for constructing the geometry while ANSYS Meshing is utilized to generate the computational grid. For the current simulation, some aspects should be followed to develop the grid that achieves an accurate and converged solution [1].

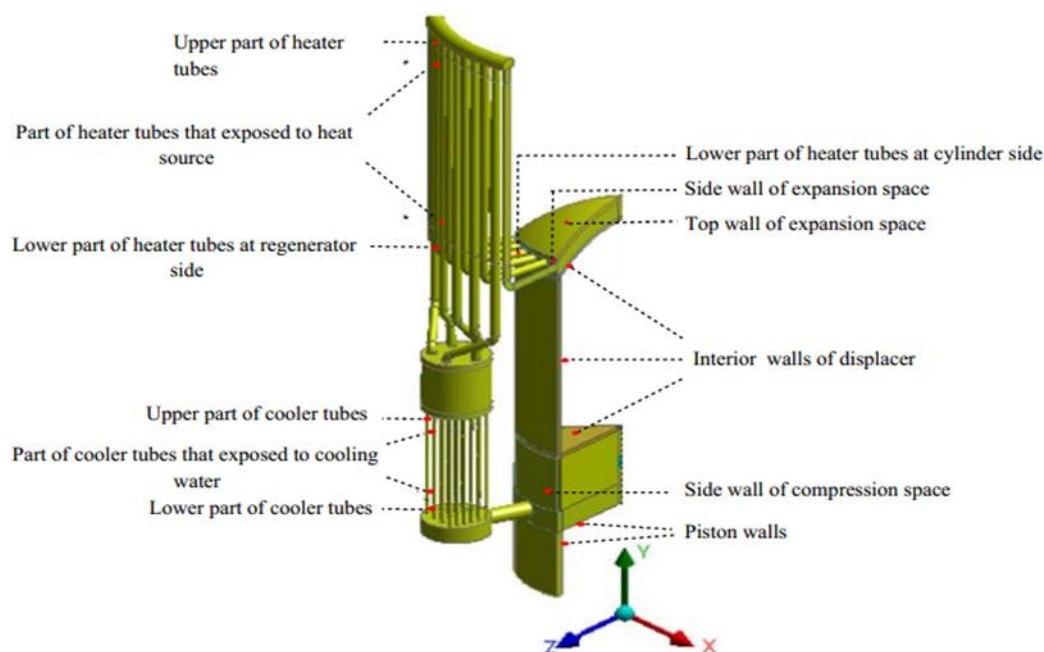


Fig. 2. Computational domain

5.2 Operating, Boundary and Initial Conditions

The operating conditions and the values of the different wall temperatures applied in the current simulation are presented in Table 1 and 2, respectively. Periodic boundary conditions are applied to the faces in the azimuthal direction since only one-eighth of the physical domain is modelled. No-slip boundary conditions are applied to all walls.

The operating conditions applied in this study is presented in Table 1. As clarified from these data, the temperature of the different engine walls, except that of the cooler tubes, have not been given. Accordingly, the temperature of the walls should be assumed, but, under specific constraints. Firstly, the cycle-averaged temperature of the gas in the whole heater tubes should be maintained as 950 K. Secondly, the heat added to the engine is restricted to the heater length that is exposed to the heat source, while the other parts of the heater is modelled with a nearly zero cyclic heat transfer rate. Similarly, the temperatures of the walls of the cooler tubes are imposed. Thirdly, the temperatures of the walls of the expansion and the compression spaces are nearly equivalent to the cycle-averaged gas temperature in the corresponding space. The assumption of isothermal wall boundary

temperature for these spaces is justified by the high thermal inertia of the solid material compared to that of the gas. Finally, the temperature of the other walls of the engine is considered to follow a linear distribution. Several trials are conducted to fulfil the operating conditions under these constraints. The values of the assumed walls temperatures, applied in the current simulation, are illustrated in Table 2. Periodic boundary conditions are applied to the faces in the azimuthal direction since only one-eighth of the physical domain is modelled. No-slip boundary conditions are applied to all walls.

Table 1
Operating condition of GPU-3 Stirling engine

Working fluid	Hydrogen
Engine speed	3500 rpm
Mean pressure of compression space	6.92 MPa
Average gas temperature in heater tubes	950 K
Metal-wall temperature of cooler tubes	293 K

Table 2
Temperature values of different walls of GPU-3 Stirling engine

Name	Temperature(K)
Top wall of expansion space	870
Side wall of expansion space	805
Side wall of compression space	325
Walls of piston	305
Interior walls of displacer	Adiabatic
Walls of upper part of heater tubes	995
Walls of a part of heater tubes that are exposed to heat source	1090
Walls of lower part of heater tubes (cylinder side)	1025
Walls of lower part of heater tubes (regenerator side)	975
Walls of upper part of cooler tubes	315
Walls of a part of cooler tubes that are exposed to cooling water	293
Walls of lower part of cooler tubes	307

Under the current setup, the initial pressure is considered as 5.5 MPa. The initial pressure is selected based on several iterations so that it is slightly higher than the cycle-minimum pressure.

5.3 Solution Scheme

The governing equations are discretized and solved using a finite volume-based solver, ANSYS FLUENT (V14.5). The solution parameters used in this simulation is illustrated in Table 3. Several techniques can be followed for speeding up the convergence of the calculation, as documented in the previous work [1].

The reciprocating motion of the displacer and the piston and, consequently, the moving and deforming volumes are modeled using the dynamic mesh technique. In order to impose the motion of the piston and displacer in the model, a special User Defined Functions (UDFs) is linked to FLUENT [1]. Meanwhile, the grid layering method is used for executing the mesh deformation.

Table 3

Solution parameters

Name	Solution Parameters
Solver type	Transient, pressure-based
Velocity formulation	Absolute
Pressure-velocity coupling	SIMPLEC
Porous media formulation	Superficial velocity approach
<u>Spatial discretization:</u>	
Gradient of transport quantities on cell faces	Least squares cell based
Pressure term	Standard
Continuity, momentum and turbulence quantities	Second-order upwind
Temporal derivatives discretization	First-order implicit
Realizable k-ε model with enhanced wall treatment Constants	$C_2=1.9, \sigma_k=1.0, \sigma_\epsilon=1.2, Pr_t=0.85$
<u>Under-relaxation factors:</u>	
Pressure	0.3
Momentum	0.7
Density, energy, turbulence quantities	0.9

The heat transfer and flow resistance coefficients should be defined in the porous media model. These coefficients are empirically obtained using the data of Tew *et al.*, [32]. Initially, at NASA Lewis Research Centre, steady state flow tests were made on the regenerators of the GPU-3 engine. From these tests, the pressure drop versus the mass flow rate was evaluated. The tests were run with air at mass flow rates that gave approximately the same Reynolds number as actually occur in the engine. The data given from NASA experiments is extrapolated to the low Reynolds number range, below 50, using the wire-screen data from kays and London [35]. Afterwards, Tew *et al.*, [32] represented these data in the form of friction factor, C_f , as a function of Reynolds number, Re , as shown in Figure 3. These data can be fitted to the two-parameter Ergun form [47], the following correlation can be obtained:

$$C_f = \frac{7.100877}{Re} + 0.567742 \quad (6)$$

From this correlation, the resistance coefficients of the porous media model $1/\alpha$ and C_2 can be obtained as $6.0183 \times 10^9 \text{ m}^{-2}$ and $1.2702 \times 10^4 \text{ m}^{-1}$, respectively [1]. With respect to the heat transfer characteristics within the regenerator, Tew *et al.*, [32] recommended the experimental results of Walker and Vasishta [48]. Their tests were performed on a regenerator of 79x79 wire/cm density and of 0.005 cm wire diameter. These specifications are close to the regenerator of the GPU-3 engine. Figure 4 illustrates the relationship between Nusselt number, Nu , and Reynolds number, Re , for the results obtained by Walker and Vasishta. By fitting these results to a two-coefficient equation form, the Nusselt number-Reynolds number correlations are obtained

$$\text{For } Re \geq 25 \quad Nu = 0.0738 Re + 2.9446 \quad (7)$$

$$\text{For } Re < 25 \quad Nu = 0.2022 Re - 0.3534 \quad (8)$$

Then, the heat transfer coefficient for the solid/fluid interface, h_{fs} , can be calculated as:

$$h_{fs} = \frac{Nu K_f}{d_h} \quad (9)$$

A UDF is used to define the heat transfer coefficient, h_{fs} , through each time step of the solution time.

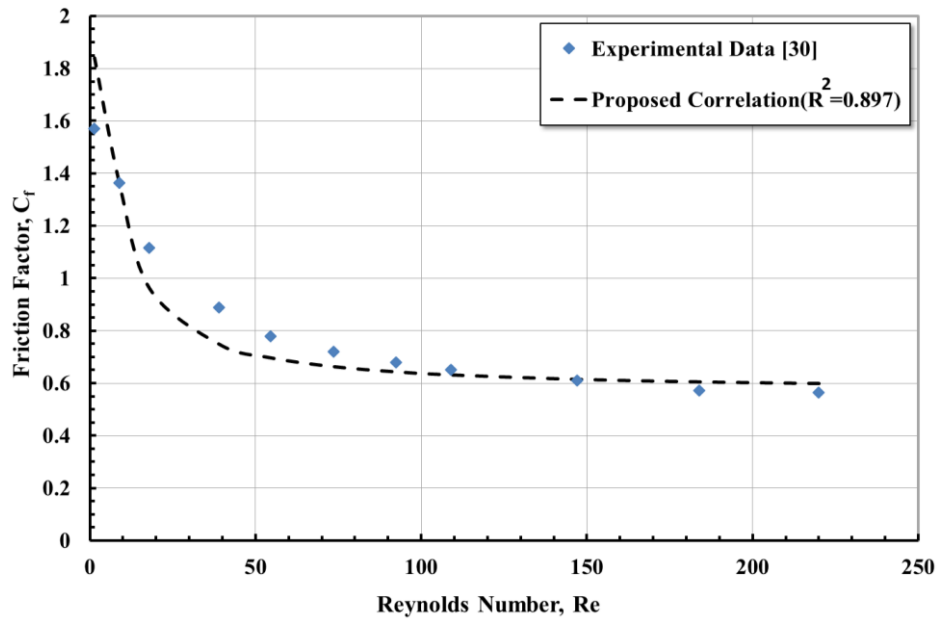


Fig. 3. Friction factor versus Reynolds number for GPU-3 regenerator

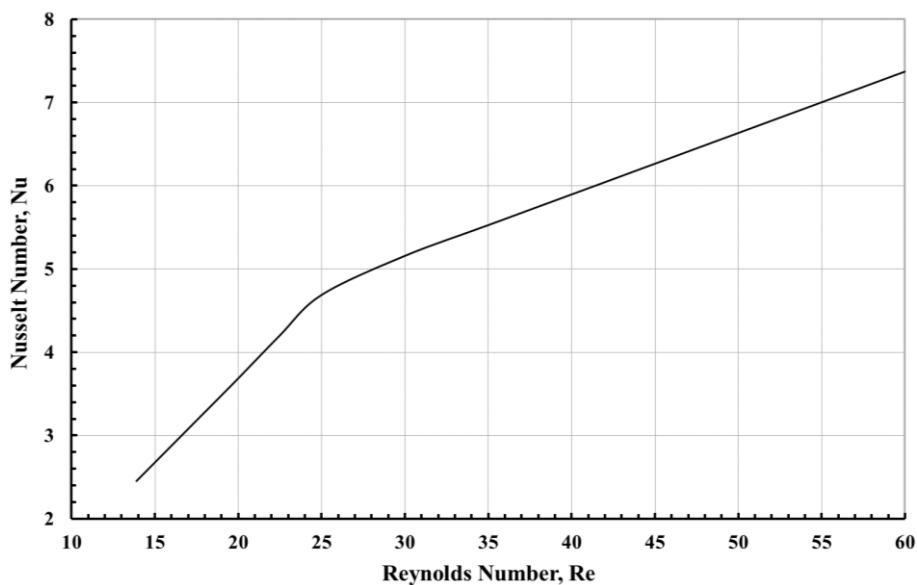


Fig. 4. Nusselt number versus Reynolds number for GPU-3 regenerator [48]

In order to obtain an accurate solution with a reasonable computational cost, dedicated independency studies are performed for the grid and time step sizes. Three different grid densities are considered, and these include 1.8×10^6 , 3.1×10^6 , and 4.3×10^6 cells. It is found that the differences in the predictions of the cycle-averaged compression space pressure between the fine and medium grids are less than 2%. Hence the medium grid is selected for this study. Furthermore, three-time step sizes are considered and, these include 7.3×10^{-5} s, 5.5×10^{-5} s and 3.06×10^{-5} s. The medium time step size is used due to its close predictions with the fine time step size, but, with a smaller computational time.

The residuals of the transport equations are monitored to ensure the convergence of the solution. The convergence criteria are set so that the residuals reach below 1×10^{-6} for the energy equations and below 1×10^{-3} for the other equations. In order to eliminate the discrepancies resulting from the initial conditions and to attain the steady-state solution, the simulations are carried out until the deviation in the cycle-averaged gas temperature between two subsequent cycles reaches below 1% for all the subdomains. Typically, six cycles are needed in order to obtain a steady state solution under the current setup. Based on a system with 16 GB memory and Core i7-6700 CPU processor with a base frequency of 3.4GHz, each complete cycle of the engine requires about 31.5h to be simulated.

5.4 Model Validation

The predictions of the current model is validated against the experimental results [49] over a range of the GPU-3 engine operating conditions. The comparison is based on the indicated power only. Since it is proved that the power developed is more sensitive to the model accuracy than the other performance parameters, such as the efficiency [1]. Figure 5 displays the validation of the power results at the maximum and minimum operating pressures of 6.92 and 2.76 MPa, respectively and over a wide range of the rotational speeds. The comparison indicates that the current CFD results have a close agreement with the experimental results over the tested operating range. The average deviation in the current results compared with the experimental ones is about 4%.

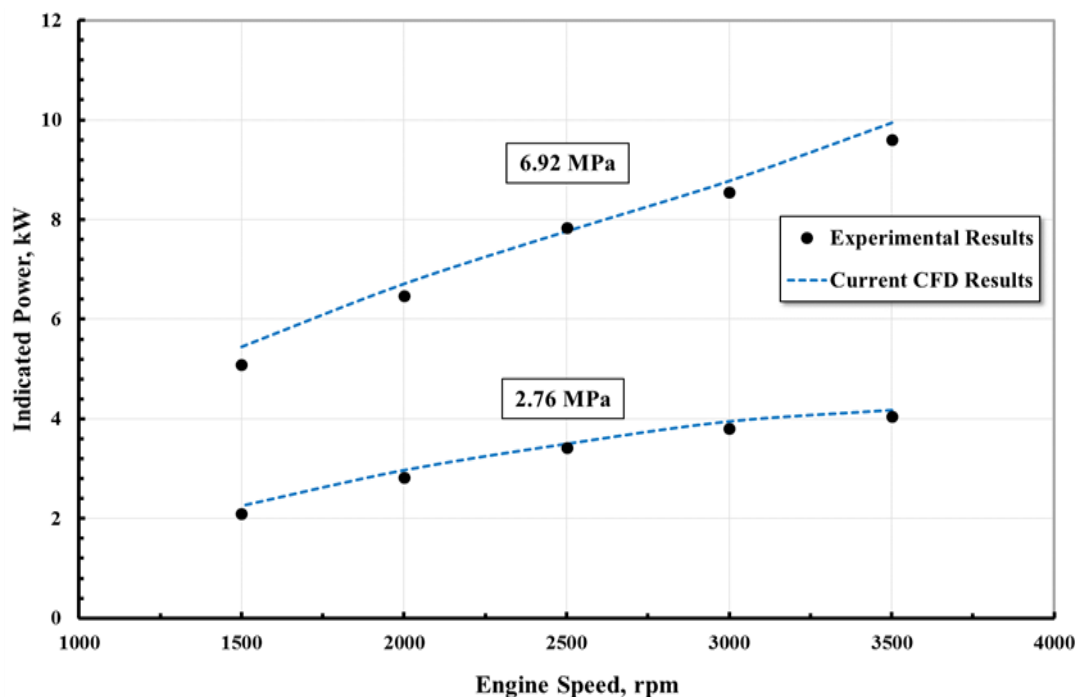


Fig. 5. Comparison of indicated power of GPU-3 Stirling engine between current CFD and experimental results at two mean operating pressures

6. Results and Discussion

In this section, the losses-related phenomena along with the method of calculating each loss are firstly addressed. Afterwards, comprehensive energy and exergy analyses of the GPU-3 Stirling engine are presented. Here, it should be referred to the importance of reviewing the comprehensive description of the cyclic fluid flow field within the GPU-3 engine presented in Ref. [1]. This significantly helps in understanding the physical phenomena addressed in the following sections.

6.1 Losses Estimation

6.1.1 Hysteresis loss

As the hysteresis loss takes place within the working spaces and the manifolds of the Stirling engine, it will be discussed within these components in the following subsections.

6.1.1.1 Working spaces

As mentioned previously, the hysteresis loss occurs due to the heat interaction between the working gas and the walls of these spaces. So, this interaction throughout the cycle should be studied within the compression and expansion spaces. In the beta-type Stirling engine, the flow jetting within the expansion space is coming from the appendix gap and the heater tubes. While, within the compression space, the flow jets come from the cooler-end duct and the appendix gap [1]. Figure 6 shows the effects of these flow jetting on the convective heat transfer coefficient at the boundaries of the expansion and compression spaces. Here, the local directive heat transfer coefficient (DHTC) is used to indicate the convective heat transfer. The DHTC is similar in its magnitude to the value of the traditional heat transfer coefficient. However, the sign of the DHTC identifies the direction. The positive sign is associated with the heat transfer direction from the solid walls towards the fluid region and vice versa.

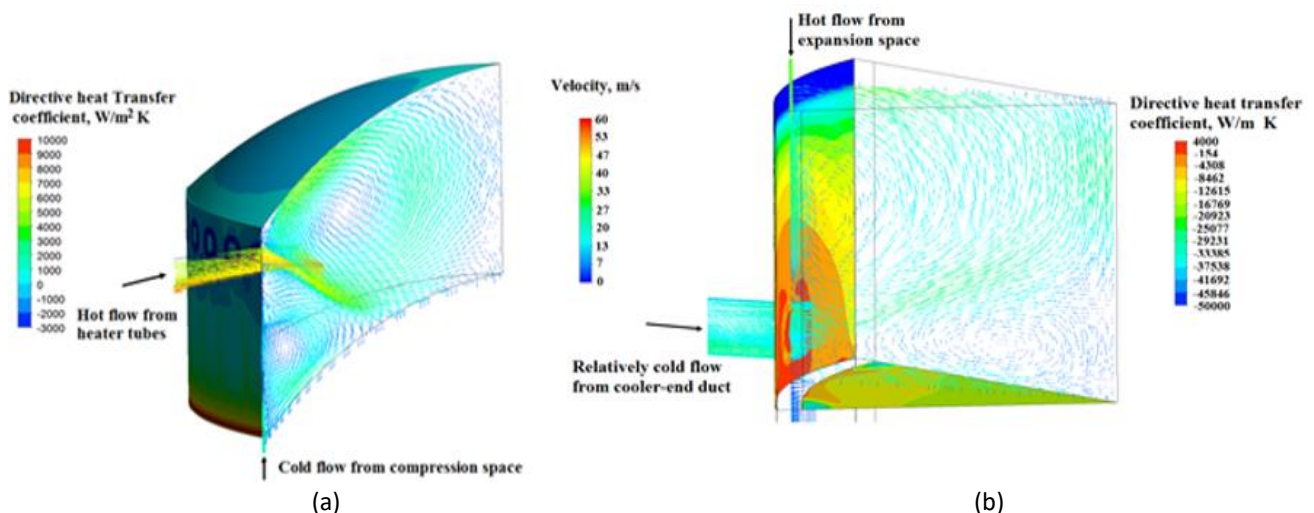


Fig. 6. Effect of flow jetting on local directive heat transfer coefficient (DHTC) at walls of (a) expansion space at $\theta = 180^\circ$ (b) compression space at $\theta = 0^\circ$

As shown in Figure 6(a), here are two counter-rotate vortices, so-called tumbles, associated with the flow jetting from the appendix gap and heater within the expansion space. The heat interaction between these tumbles and the walls of the expansion spaces is affected by the jetting process, the mixing process between the two tumbles, and the consequent heat dissipation. On the other side, the two jets that flows from the appendix gap and the cooler-end duct forms a single tumble vortex in the compression space, as displayed in Figure 6(b).

By investigating the effect of these jets throughout the cycle [1], the variation of the instantaneous convective heat transfer rates at the walls of the spaces can be estimated, as seen in Figure 7. It can be demonstrated that the convective heat transfer rates is significantly enhanced during the first part of the expansion stroke of the expansion space, i.e., period from 90° to 180° . While, the peak enhancement of this rate occurs during the period from 245° to 360° which also

represents the first part of the expansion stroke of the compression space. With respect to this figure, the cyclic convective heat transfer rate from the walls of the compression and expansion spaces can be calculated according to Eq. (2). These values represent the hysteresis losses from the working spaces. Here, it is worthy mentioned that the hysteresis loss occurs mainly within the working spaces due to the flow jetting during the first part of the expansion strokes.

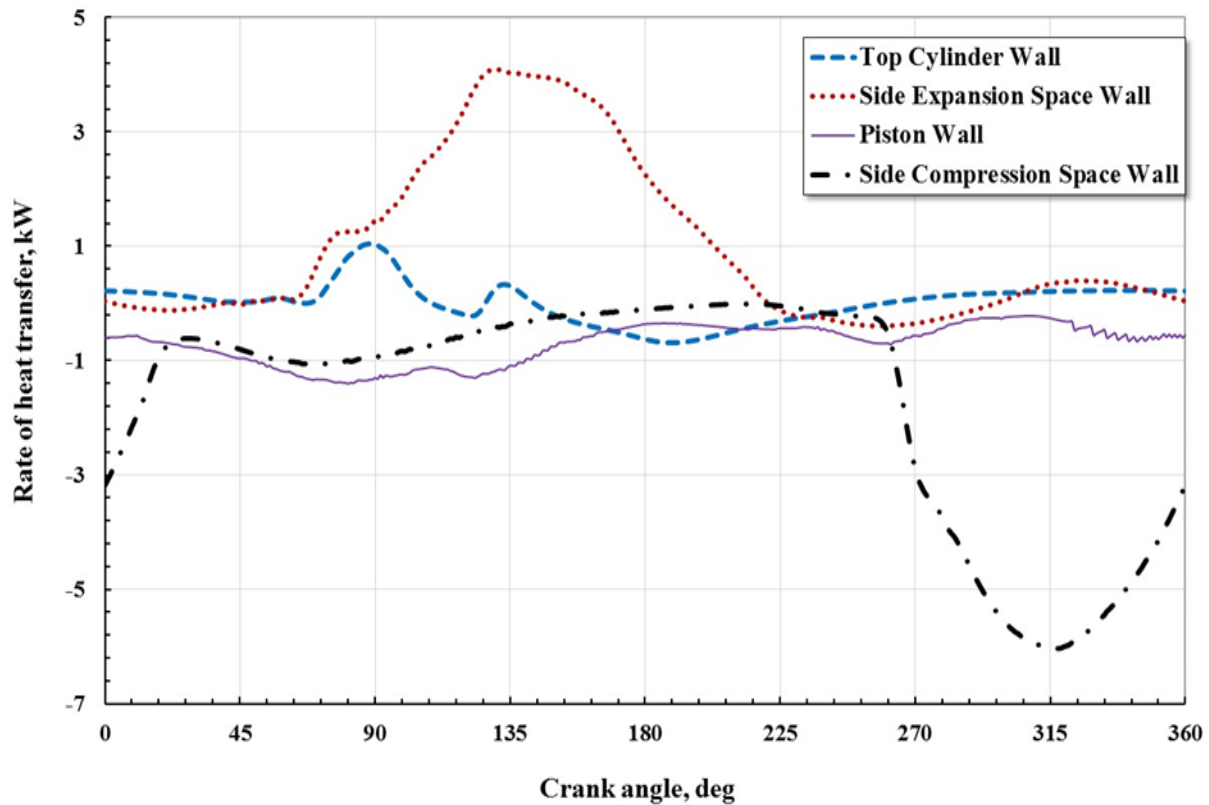


Fig. 7. Instantaneous convective heat transfer rates at the walls of expansion and compression spaces over one cycle versus crank angle

6.1.1.2 Manifolds of hot and cold spaces

In general, the manifolds of the Stirling engine are divided into two main categories. These are the manifolds of the hot spaces and that of the cold spaces. Here, the hot space manifolds include the heater header and the parts of the heater tubes that are not exposed to the heat source. Whereas the cooler-end connection and the parts of the cooler tubes that are not exposed to the cooling water are considered the manifolds of the cold space. The instantaneous convective heat transfer rate in the engine manifolds as a function of the crank angle are illustrated in Figure 8.

As mentioned by El-Ghafour *et al.*, [1], the cycle starts when most of the fluid amount exists in the cold space. The hot fluid continuously flows from the expansion to the compression space, however, with small mass flow rate. This causes the observed reduction in the convective heat transfer in the hot manifolds till about 110°. This behavior is attributed to the direct proportional relation between the mass flow rate, consequently the flow Reynolds number, and the convective heat transfer rate. However, the flowing of this hot flow through the cold manifolds causes a contradicting effect. As, a large rate of the convective heat loss in the cold manifolds is observed. After the reversal of the flow direction, a marked increase in the convective heat transfer rate in the hot manifolds occurs. This is due to passing of enhanced rates of the cold flow through the manifolds.

It causes, on the other hand, a rapid decrease in the heat transfer rate in the cold manifolds. When the flow direction is reversed again, an opposite trend of the heat transfer rate is noticed in the hot and cold manifolds. The maximum increase in the convective heat transfer rate for the hot manifolds occurs in the period from 225°-333°. As the slightly hot fluid flows at large mass rates from the expansion space to the compression one. Meanwhile, this fluid loses heat at small rates in the cold manifolds. From Figure 8, the hysteresis loss through the engine manifolds can be estimated according to Eq. (2).

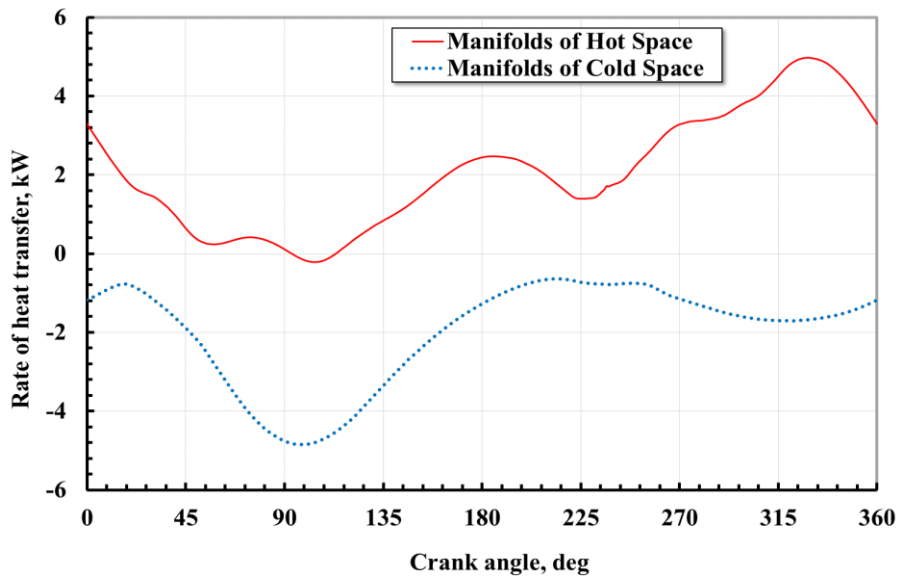


Fig. 8. Instantaneous convective heat transfer rates in the manifolds of hot and cold spaces versus crank angle

6.1.2 Regenerator thermal loss

A schematic representation of the heat interaction between gas and solid matrix within the regenerator during the hot and cold flow periods is shown in Figure 9.

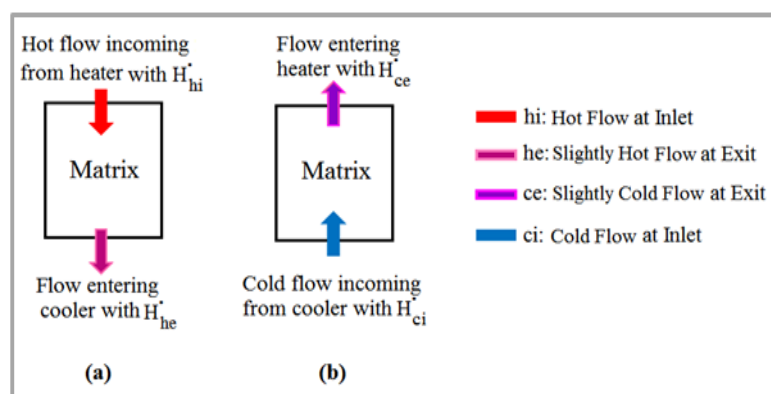


Fig. 9. Instantaneous heat transfer coefficient and flow Reynolds number within regenerator versus crank angle

Generally, the heat exchange between the gas and the matrix within regenerator can be obtained from the change in the enthalpy flow rate of the fluid entering and exiting the regenerator. The instantaneous enthalpy flow rate of the fluid at a specific cross-sectional area, \dot{H}^{\cdot} , is determined by

$$\dot{H} = \int_{\text{area}} \rho u C_p(T) (T - T_{\text{ref}}) dA_c \quad (10)$$

The instantaneous enthalpy flow rate of the gas at both ends of the regenerator, at heater/regenerator and cooler/regenerator interfaces, along with the net rate between both ends is shown in Figure 10. The positive values correspond to the heat transfer from the matrix to the gas and vice versa. In this regard, the thermal heat loss through the regenerator, $\dot{Q}_{\text{loss},r}$, can be determined. It represents the cyclic integration of the instantaneous net enthalpy flow rate, \dot{H}_{net} , between the two ends of the regenerator as

$$\dot{Q}_{\text{loss},r} = \frac{\omega_r}{2\pi} \oint \dot{H}_{\text{net}} dt \quad (11)$$

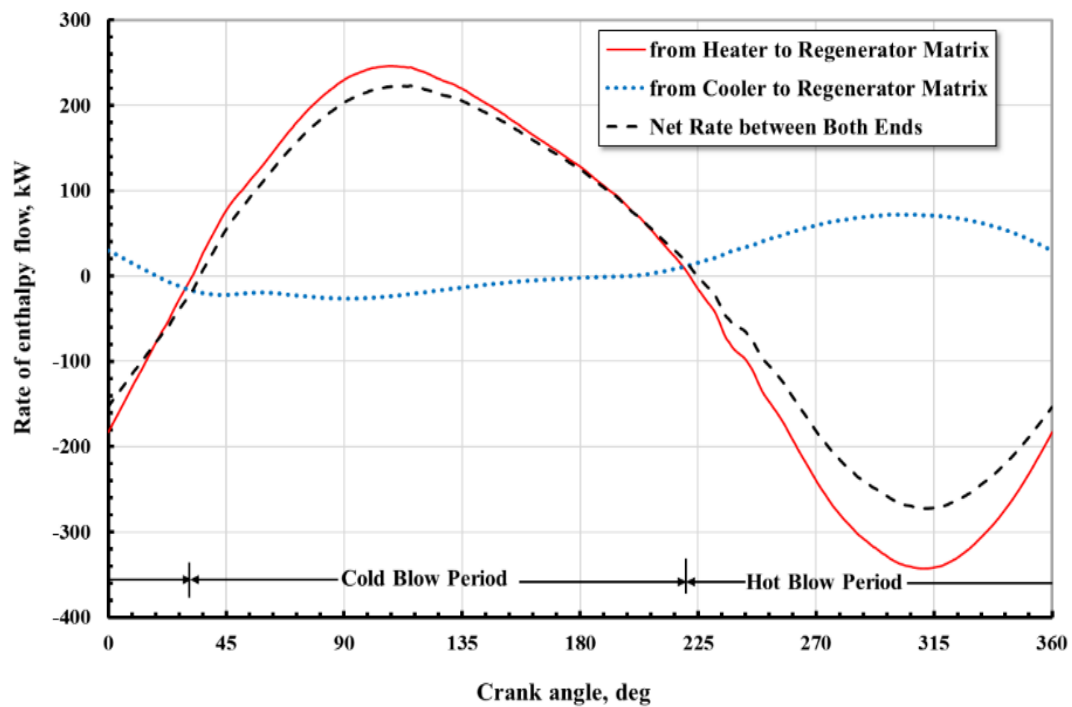


Fig. 10. Instantaneous enthalpy flow rate of gas at both sides of regenerator along with net enthalpy flow rate between the both ends versus crank angle

This non-ideal operation of the regenerator is attributed to several imperfect issues. The geometrical and material characteristics of the matrix as well as the time allowed for heat transfer significantly affects the storing and recovering of heat in the regenerator. Also, the axial conduction loss through the regenerator matrix, the convective heat loss to the walls of the regenerator housing and the swing loss due to the temperature oscillation are other effects that cause the non-ideal operation.

Although there are several definitions for the effectiveness of the regenerator, as mentioned previously in section 1.2, the authors find that it is reasonable to use another definition. This is the ratio of the enthalpy gained by the gas during the cold blow period to the maximum possible enthalpy that could be stored in the regenerator during the hot blow period. Accordingly, the effectiveness, ϵ_r , can be calculated as

$$\epsilon_r = \frac{\int_{\text{CBP}} (\dot{H}_{\text{ce}} - \dot{H}_{\text{ci}}) dt}{\int_{\text{HBP}} (\dot{H}_{\text{hi}} - \dot{H}_{\text{ci}}) dt} \quad (12)$$

where CBP and HBP refer to the cold and hot blow periods, respectively. According to Eq. (11), the effectiveness of the current regenerator equals 0.704.

6.1.3 Shuttle heat transfer and enthalpy pumping losses

Actually, the heat flow through the displacer as well as the fluid flow within the appendix gap are considered as the most complex phenomena occurring in Stirling engines. A comprehensive description of the fluid flow through the appendix gap over the whole cycle was presented by El-Ghafour *et al.*, [1]. With respect to these results, the enthalpy pumping loss through the appendix gap can be calculated. Generally, the instantaneous enthalpy flow rate at the inlet of the appendix gap, H_{ag} , can be calculated as

$$H_{ag} = 2\pi \int_{R_d}^{R_d+J} (\rho u C_p(T)(T - T_{ref})) r dr \quad (13)$$

The instantaneous variation of the enthalpy flow rate of the gas entering the appendix gap from the expansion space over the cycle is displayed in Figure 11. The positive values indicate the gas flow from the expansion space to the compression one and vice versa. Also, the figure shows the pressure difference between the expansion and compression spaces. From this figure, it is demonstrated that the pressure difference between the expansion and compression spaces is the main driver for the gas flow through the appendix gap. This clarifies from the matching between the two trends except in period from 63.9° to 109.8°. Despite the increase in the pressure difference during this period, the mass flow rate from the compression to the expansion spaces significantly decreases. This is attributed to another parameter affecting the mass flow through this gap. The displacer direction is reversed during this period and, hence, allowing for a gradual opening for the heater tubes to pour the fluid within the expansion space [1]. This partially obstructs the flow induced from the compression space to the expansion one through the appendix gap. Generally, the matching between the enthalpy flow and the pressure difference trends confirms the prevailing of the pressure difference effect over the other effects: axial temperature gradient, displacer motion and heat exchange between the displacer walls and appendix gap.

The enthalpy pumping loss, $Q_{loss,ag}$, is estimated from the cyclic integration of the instantaneous enthalpy flow rate at the inlet of the appendix gap, H_{ag} , as

$$Q_{loss,ag} = \frac{\omega_r}{2\pi} \oint H_{ag} dt \quad (14)$$

In order to estimate the shuttle heat loss, the instantaneous heat conduction rate at the displacer top wall should be calculated as

$$Q_{cond,d} = \int_{area} -K_f \frac{\partial T_f}{\partial n} |_{DTW} dA \quad (15)$$

DTW denotes to displacer top wall. The instantaneous variation of the heat conduction rate at the displacer top wall throughout the cycle is presented in Figure 12. Hence, the shuttle heat loss, $Q_{shuttle}$, can be determined

$$Q_{shuttle} = \frac{\omega_r}{2\pi} \oint Q_{cond,d} dt \quad (16)$$

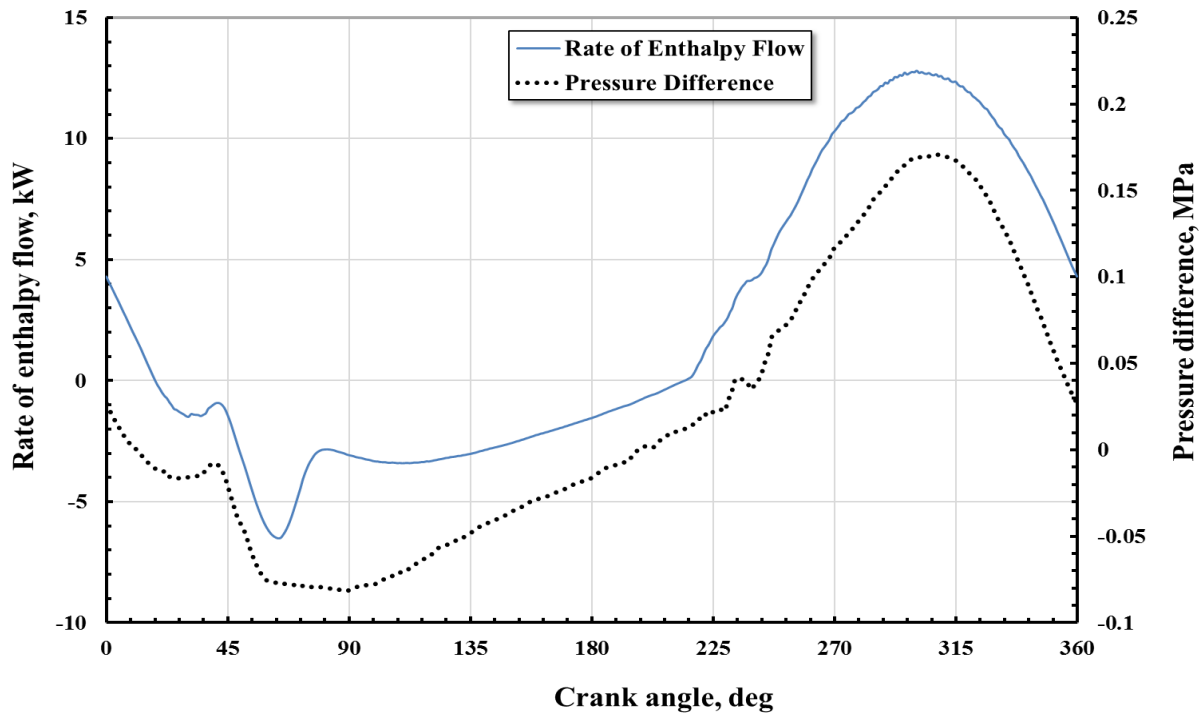


Fig. 11. Instantaneous enthalpy flow rate of fluid entering the appendix gap from expansion space and pressure difference between expansion and compression spaces versus crank angle

Regarding to Figure 12, it can be demonstrated that the heat conduction rate is significantly enhanced during the period from 90° - 180° . During this period, the hot gas coming from the heater tubes flows into the expansion space, as noticed from the figure. Accordingly, the exposure of the displacer top wall to this jet of hot gas during the expansion stroke of the expansion space essentially increases the shuttle heat loss.

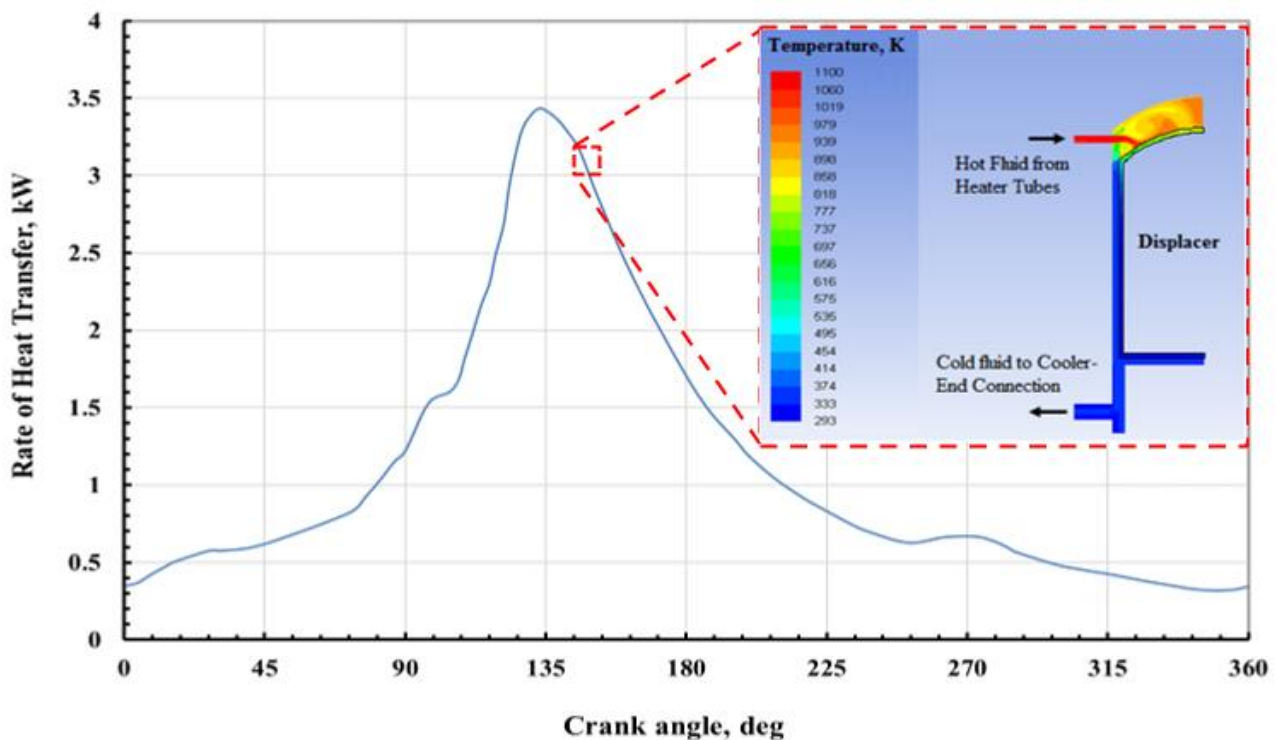


Fig. 12. Instantaneous conductive heat transfer rate at top wall of the displacer versus crank angle

6.1.4 Pumping loss

In order to estimate the pumping loss, the pressure loss in each component of the engine is firstly calculated. Figure 13 illustrates the instantaneous variation of the pressure loss through the engine components; heater and its header, regenerator as well as cooler and its end-connection. Here, the pressure loss at the entrance and the exit of each component is also included. The sign indicates the direction as the positive sign corresponds to the flow direction from the expansion space to the compression one and vice versa.

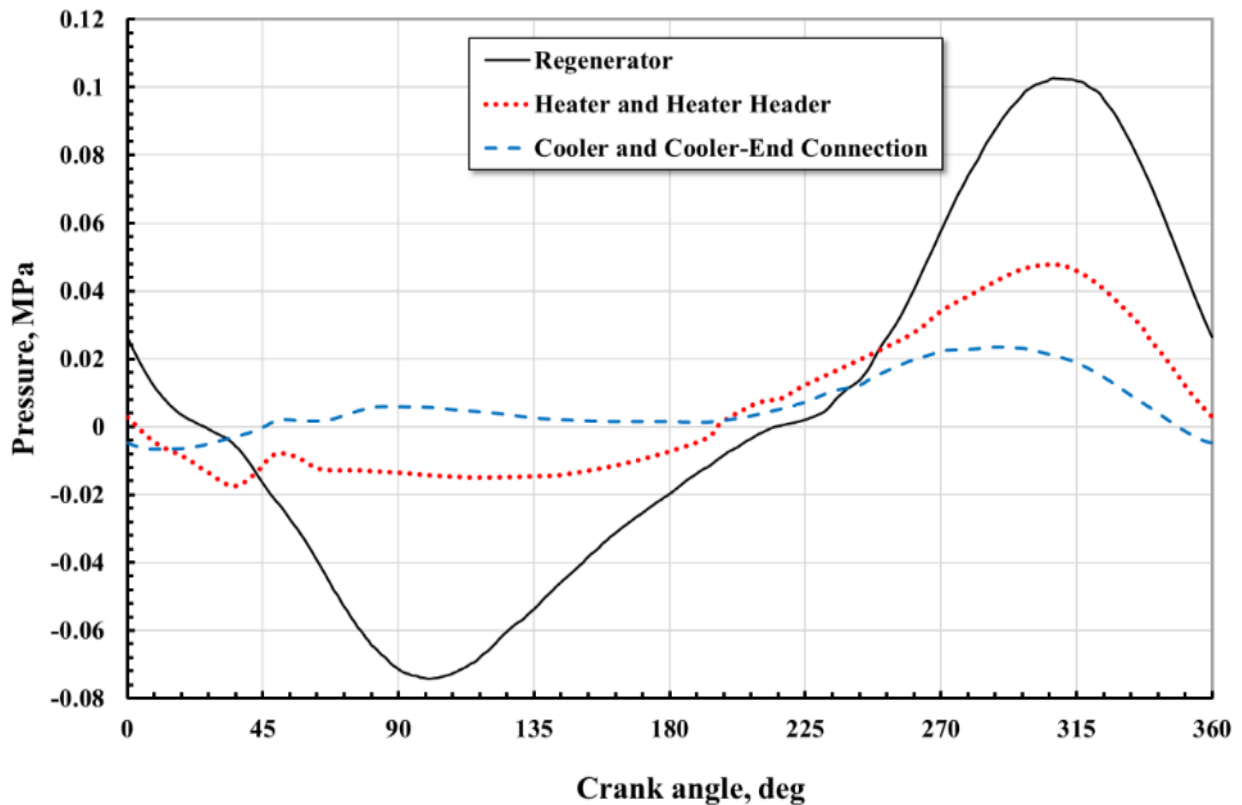


Fig. 13. Instantaneous pressure loss through regenerator, heater and header as well as cooler and cooler-end connection versus crank angle

As observed from this figure, the pressure loss in the regenerator is the main contributor of the total pressure loss within the engine. Meanwhile, it is noticeable that the pressure loss in the heater and its header has also a significant value. This is due to the complicated design of the heater tubes in the GPU-3 Stirling engine. Also, the pressure loss in the cooler tubes and its end-connection represents a considerable value. These results, about the heater and cooler tubes, conflict with the results of Babaelahi and Sayyaadi [41] and Tlili *et al.*, [51]. The pumping loss can be calculated according the following equation

$$P_{\text{pumping}} = \frac{|\Delta p| \dot{m}}{\rho_m} \quad (17)$$

where ρ_m is the mean value of the density through each component respectively.

6.1.5 Power loss due to piston finite speed

Figure 14 displays the variations of the average pressure within the compression space, expansion space and on the piston wall as functions of the crank angle over the cycle. From this figure, the power delivered to the piston surface is computed as

$$P_p = \left(\frac{\omega_r}{2\pi}\right) \oint \left(\int_{\text{piston}} p \, dA_c\right) dy \quad (18)$$

The difference between the indicated power and the piston power represents the piston finite speed power loss.

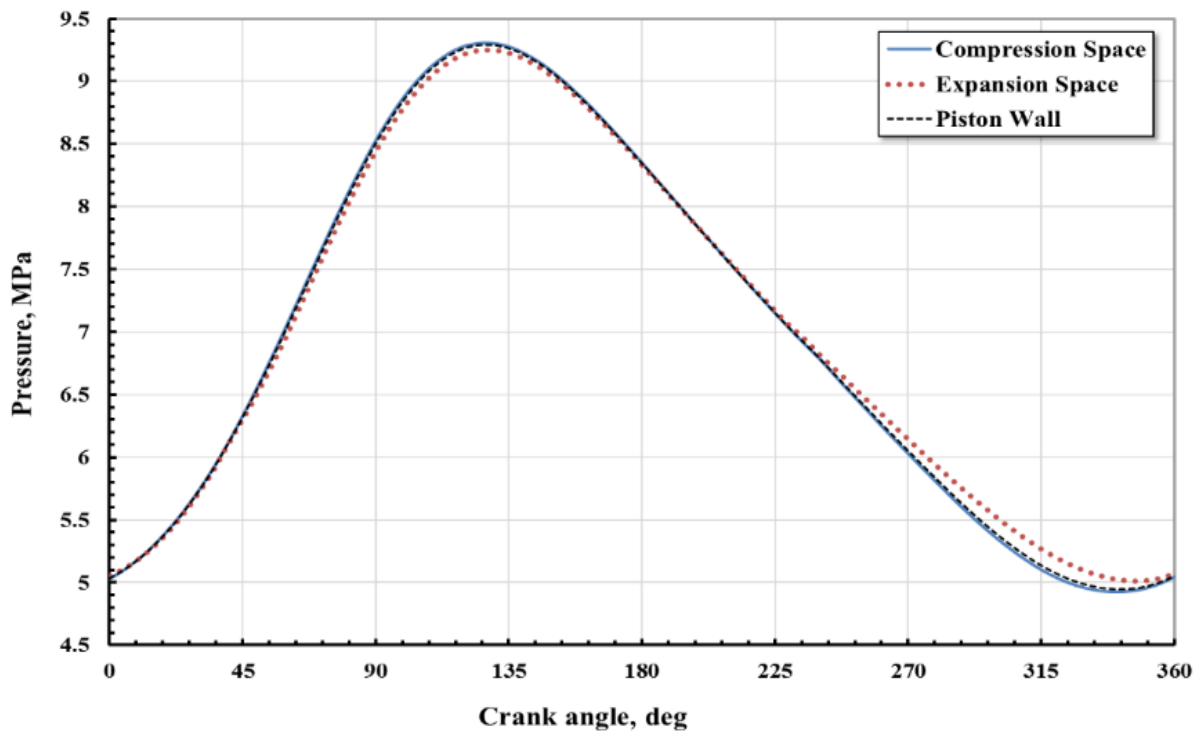


Fig. 14. Instantaneous variation of average pressure in compression; expansion spaces and on the piston wall versus crank angle

6.2 Energy and Exergy Analyses of GPU-3 Stirling Engine

The p-V diagram of the expansion and the compression spaces is displayed in Figure 15. Therefore, the indicated power, P_{ind} , of the GPU-3 engine can be estimated according to Eq. (1).

The instantaneous variations of both the added heat rate to the heater tubes and the rejected heat rate out of the cooler tubes are illustrated in Figure 16. Accordingly, the cyclic rate of heat addition in the heater and the heat rejection out of the cooler can be calculated using Eq. (2).

The energy balance representation for the GPU-3 Stirling engine is shown in Figure 17(a). As demonstrated from this balance, the regenerator thermal loss and pumping power represent the largest part of the engine losses by about 9.2% and 7.5% of the heat input, respectively. The thermal efficiency of the GPU-3 Stirling engine, based on the power piston, is 36.6%.

Figure 17(b) represents the exergy loss, %, within each component of the GPU-3 engine. The engine is divided into six components: expansion space, compression space, appendix gap, heater with its header, regenerator in addition to cooler with its end connection.

As demonstrated from this figure, the exergy loss within the regenerator is the largest part and represents more than one-third of the total exergy loss within engine. Accordingly, the effective redesign for the regenerator is expected to highly increase the overall engine performance. Here, it is worth noting the high exergy loss within the cold space, the compression space and the cooler with its end connection, compared with the hot space. This indicates the importance of redesigning this component as well.

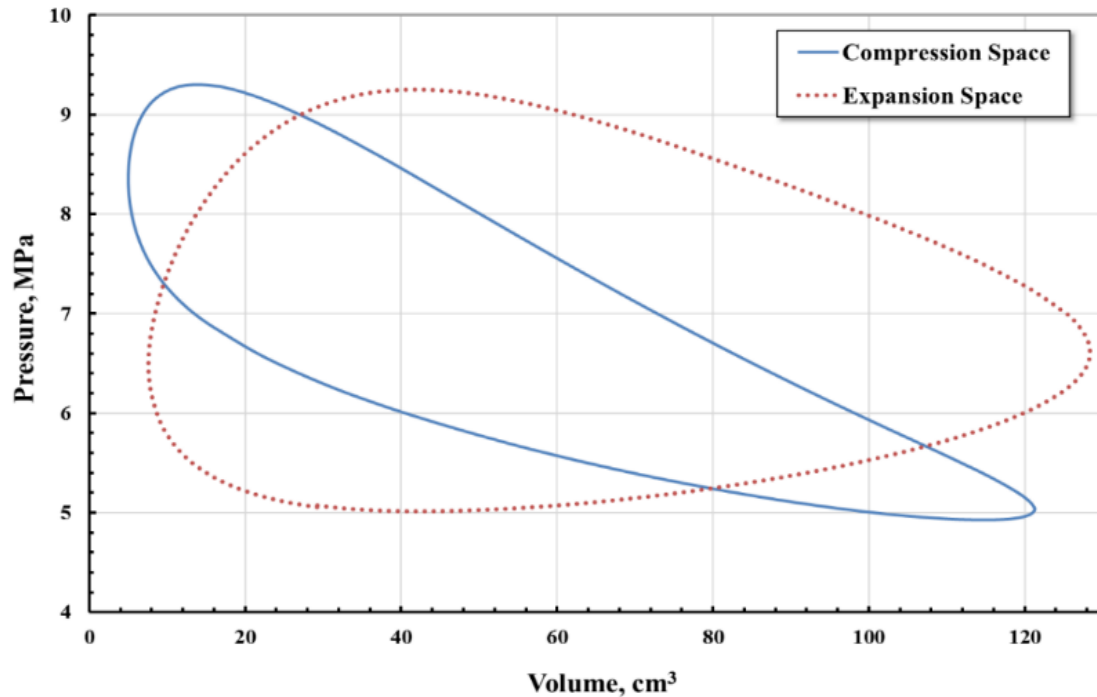


Fig. 15. p-V diagrams of expansion and compression spaces of GPU-3 Stirling engine

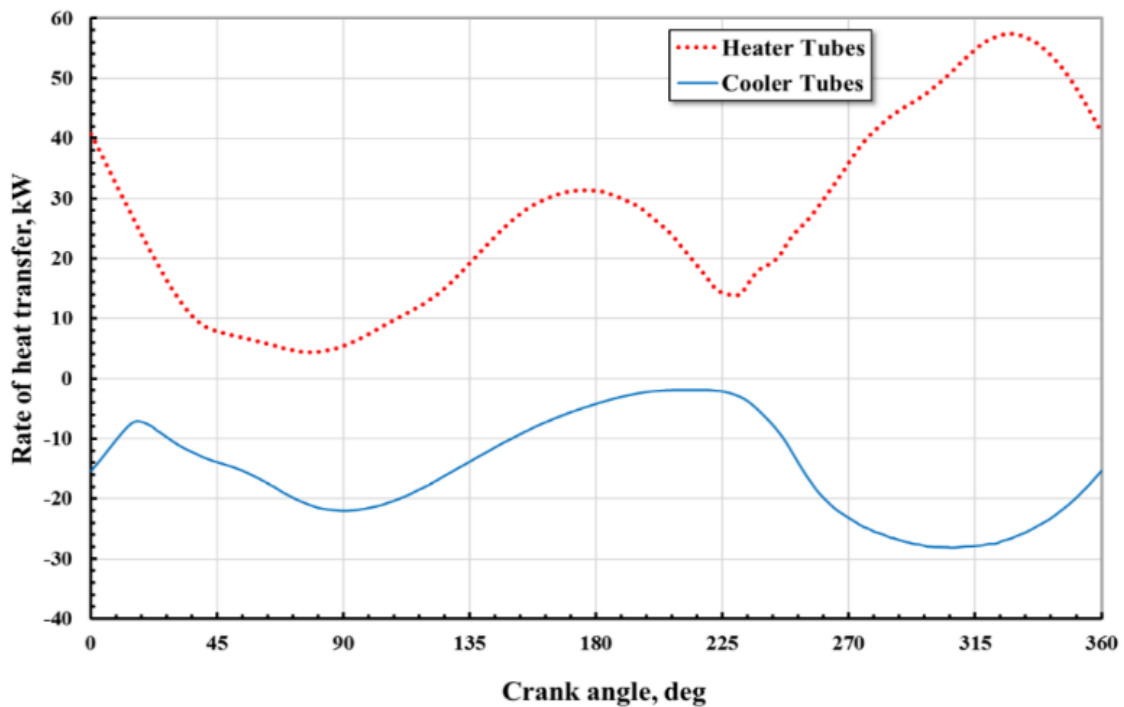


Fig. 16. Instantaneous added heat rate to the heater tubes and rejected heat rate out of the cooler tubes versus crank angle

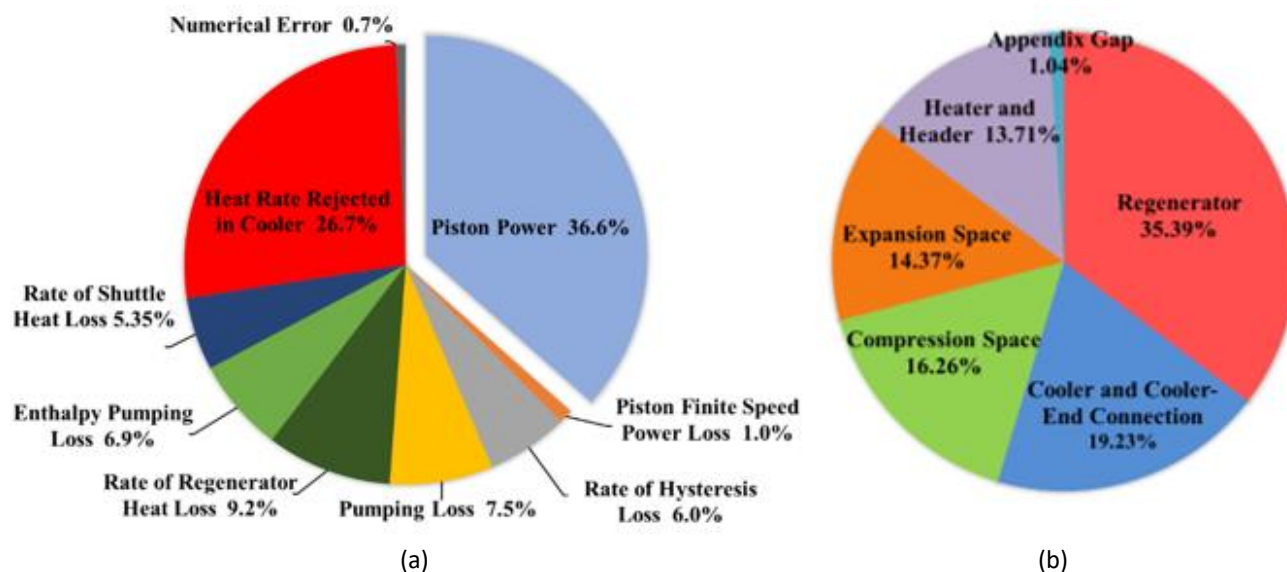


Fig. 17. (a) Energy balance and (b) Exergy loss, %, within each component of GPU-3 Stirling engine

7. Conclusion

A comprehensive characterization of the Stirling engine losses with the aid of the CFD approach is presented. Firstly, a detailed description of the losses-related phenomena along with the method of calculating each type of loss are addressed. Secondly, an energy analysis of the Stirling engine is carried out in order to specify the impact of each type of losses on the performance. Finally, the design effectiveness of each component of the GPU-3 Stirling engine is investigated using an exergy analysis. The results reveal that

- i. Avoid excessively large white space borders around your graphics;
- ii. The hysteresis loss within the working spaces occurs mainly due to the impinging effect associated with the tumble vortices released from the flow jetting during the expansion strokes within working spaces.
- iii. A new definition for the regenerator effectiveness is presented to assess the quality of the heat storage and recovery processes. The definition takes in consideration the different type of losses occurred in regenerator besides the time of heat interaction between the gas and the matrix.
- iv. A highly matching between the flow leakage through the appendix gap and the pressure difference between the working spaces throughout the cycle is observed. This confirms the prevailing of the pressure difference effect over other effects: axial temperature gradient, displacer motion and heat exchange between the appendix gap and displacer walls.
- v. The energy analysis demonstrates that the regenerator thermal loss and the pumping power represent the largest part of the Stirling engine losses by about 9.2% and 7.5% of the heat input, respectively.
- vi. The exergy losses within the regenerator and cold space are the largest values among the other components by about 35.39% and 35.49%, respectively. These components need to be redesigned.

References

- [1] El-Ghafour, S. A., M. El-Ghandour, and N. N. Mikhael. "Three-dimensional computational fluid dynamics simulation of stirling engine." *Energy conversion and management* 180 (2019): 533-549. <https://doi.org/10.1016/j.enconman.2018.10.103>
- [2] Alfarawi, S., R. Al-Dadah, and S. Mahmoud. "Influence of phase angle and dead volume on gamma-type Stirling engine power using CFD simulation." *Energy Conversion and Management* 124 (2016): 130-140. <https://doi.org/10.1016/j.enconman.2016.07.016>
- [3] Chen, Wen-Lih, King-Leung Wong, and Yu-Feng Chang. "A computational fluid dynamics study on the heat transfer characteristics of the working cycle of a low-temperature-differential γ -type Stirling engine." *International Journal of Heat and Mass Transfer* 75 (2014): 145-155. <https://doi.org/10.1016/j.ijheatmasstransfer.2014.03.055>
- [4] Mahkamov, K. "Design improvements to a biomass Stirling engine using mathematical analysis and 3D CFD modeling." (2006): 203-215. <https://doi.org/10.1115/1.2213273>
- [5] Ahmed, Fawad, Hulin Huang, Shoaib Ahmed, and Xin Wang. "A comprehensive review on modeling and performance optimization of Stirling engine." *International Journal of Energy Research* (2020).
- [6] Malroy, Eric Thomas. "Solution of the Ideal Adiabatic Stirling Model with Coupled First Order Differential Equations by the Pasic Method." PhD diss., Ohio University, 1998.
- [7] Bumataria, Rakesh K., and Nikul K. Patel. "Stirling engine performance prediction using Schmidt analysis by considering different losses." *IJRET: International Journal of Research in Engineering and Technology eISSN* (2013): 2319-1163. <https://doi.org/10.15623/ijret.2013.0208067>
- [8] Xiao, Gang, Umair Sultan, Mingjiang Ni, Hao Peng, Xin Zhou, Shulin Wang, and Zhongyang Luo. "Design optimization with computational fluid dynamic analysis of β -type Stirling engine." *Applied Thermal Engineering* 113 (2017): 87-102. <https://doi.org/10.1016/j.applthermaleng.2016.10.063>
- [9] Tew Jr, Roy C. "Overview of heat transfer and fluid flow problem areas encountered in Stirling engine modeling." (1988).
- [10] Hachem, Houda, Ramla Gheith, Fethi Aloui, and Sassi Ben Nasrallah. "Numerical characterization of a γ -Stirling engine considering losses and interaction between functioning parameters." *Energy conversion and management* 96 (2015): 532-543. <https://doi.org/10.1016/j.enconman.2015.02.065>
- [11] Kornhauser, Alan Abram. "Gas-wall heat transfer during compression and expansion." PhD diss., Massachusetts Institute of Technology, 1989.
- [12] Lee, Kang P., and J. L. Smith. "Influence of cyclic wall-to-gas heat transfer in the cylinder of the valved hot-gas engine." In *From: Intersociety Energy Conversion Engineering Conference, 13th Proceedings.*, no. SAE 789195 Conf Paper. 1978.
- [13] Jeong, Eun S. "Heat transfer with oscillating pressure in reciprocating machinery." PhD diss., Massachusetts Institute of Technology, 1991.
- [14] Urieli, Israel, and David M. Berchowitz. *Stirling cycle engine analysis*. Bristol, UK: A. Hilger, 1984.
- [15] Scheck, Christopher G. "Thermal hysteresis loss in gas springs." PhD diss., Ohio University, 1988.
- [16] Willich, Caroline, Christos N. Markides, and Alexander J. White. "An investigation of heat transfer losses in reciprocating devices." *Applied Thermal Engineering* 111 (2017): 903-913. <https://doi.org/10.1016/j.applthermaleng.2016.09.136>
- [17] Timoumi, Youssef, Iskander Tlili, and Sassi Ben Nasrallah. "Design and performance optimization of GPU-3 Stirling engines." *Energy* 33, no. 7 (2008): 1100-1114. <https://doi.org/10.1016/j.energy.2008.02.005>
- [18] Sullivan, Timothy J. "NASA Lewis Stirling Engine Computer Code Evaluation." (1989).
- [19] Andersen, Stig Kildegård, Henrik Carlsen, and Per Grove Thomsen. "Numerical study on optimal Stirling engine regenerator matrix designs taking into account the effects of matrix temperature oscillations." *Energy Conversion and Management* 47, no. 7-8 (2006): 894-908. <https://doi.org/10.1016/j.enconman.2005.06.006>
- [20] Costa, S. C., Igor Barreno, Mustafa Tutar, Jon-Ander Esnaola, and Harritz Barrutia. "The thermal non-equilibrium porous media modelling for CFD study of woven wire matrix of a Stirling regenerator." *Energy conversion and management* 89 (2015): 473-483. <https://doi.org/10.1016/j.enconman.2014.10.019>
- [21] De Boer, P. C. T. "Optimal regenerator performance in Stirling engines." *International Journal of Energy Research* 33, no. 9 (2009): 813-832. <https://doi.org/10.1002/er.1516>
- [22] Baik, Jong Hoon, and Ho-Myung Chang. "An exact solution for shuttle heat transfer." *Cryogenics* 35, no. 1 (1995): 9-13. [https://doi.org/10.1016/0011-2275\(95\)90418-F](https://doi.org/10.1016/0011-2275(95)90418-F)
- [23] Mabrouk, Mohamed Tahar, Abdelhamid Kheiri, and Michel Feidt. "Displacer gap losses in beta and gamma Stirling engines." *Energy* 72 (2014): 135-144. <https://doi.org/10.1016/j.energy.2014.05.017>
- [24] Segado, M. A., and J. G. Brisson. "Appendix Gap Losses with Pressure-Driven Mass Flows." (2012).

- [25] Rios, P. A. "An approximate solution to the shuttle heat-transfer losses in a reciprocating machine." (1971): 177-182. <https://doi.org/10.1115/1.3445549>
- [26] William, R. MARTINI. "Stirling engine design manual." *Martini Engineering* (1983).
- [27] Chang, Ho-Myung, Dae-Jong Park, and Sangkwon Jeong. "Effect of gap flow on shuttle heat transfer." *Cryogenics* 40, no. 3 (2000): 159-166. [https://doi.org/10.1016/S0011-2275\(00\)00020-5](https://doi.org/10.1016/S0011-2275(00)00020-5)
- [28] Sauer, Jan, and Hans-Detlev Kuehl. "Numerical model for Stirling cycle machines including a differential simulation of the appendix gap." *Applied Thermal Engineering* 111 (2017): 819-833. <https://doi.org/10.1016/j.applthermaleng.2016.09.176>
- [29] Formosa, Fabien, and Ghislain Despesse. "Analytical model for Stirling cycle machine design." *Energy Conversion and Management* 51, no. 10 (2010): 1855-1863. <https://doi.org/10.1016/j.enconman.2010.02.010>
- [30] Pfeiffer, Jens, and Hans-Detlev Kuehl. "Review of Models for Appendix Gap Losses in Stirling Cycle Machines." *Journal of Propulsion and Power* 30, no. 5 (2014): 1419-1432. <https://doi.org/10.2514/1.B35132>
- [31] Strauss, Johannes Matthias. "Direct piston displacement control of free-piston Stirling engines." PhD diss., Stellenbosch: Stellenbosch University, 2013.
- [32] Tew, Roy C., Kent Jefferies, and David Miao. *A Stirling engine computer model for performance calculations*. Vol. 78884. Department of Energy, Office of Conservation and Solar Applications, Division of Transportation Energy Conservation, 1978.
- [33] Alfarawi, Suliman. "Thermodynamic analysis of rhombic-driven and crank-driven beta-type Stirling engines." *International Journal of Energy Research* 44, no. 7 (2020): 5596-5608. <https://doi.org/10.1002/er.5309>
- [34] Kays, William Morrow, and Alexander Louis London. "Compact heat exchangers." (1984).
- [35] Barreno, Igor, S. C. Costa, Marta Cordon, Mustafa Tutar, Idoia Urrutibeascoa, Xabo Gomez, and German Castillo. "Numerical correlation for the pressure drop in Stirling engine heat exchangers." *International Journal of Thermal Sciences* 97 (2015): 68-81. <https://doi.org/10.1016/j.ijthermalsci.2015.06.014>
- [36] Ibrahim, Mounir B., and Roy C. Tew Jr. *Stirling convertor regenerators*. CRC Press, 2011.
- [37] Chen, Norbert CJ, and Fred P. Griffin. *Effects of pressure-drop correlations on Stirling-engine predicted performance*. No. CONF-830812-52. Oak Ridge National Lab., TN (USA), 1983.
- [38] Simon, Terrence W., and Jorge R. Seume. "A survey of oscillating flow in stirling engine heat exchangers." (1988).
- [39] Hosseinzade, Hadi, and Hoseyn Sayyaadi. "CAFS: The Combined Adiabatic-Finite Speed thermal model for simulation and optimization of Stirling engines." *Energy conversion and Management* 91 (2015): 32-53. <https://doi.org/10.1016/j.enconman.2014.11.049>
- [40] Costea, M., S. Petrescu, and C. Harman. "The effect of irreversibilities on solar Stirling engine cycle performance." *Energy conversion and management* 40, no. 15-16 (1999): 1723-1731. [https://doi.org/10.1016/S0196-8904\(99\)00065-5](https://doi.org/10.1016/S0196-8904(99)00065-5)
- [41] Babaelahi, Mojtaba, and Hoseyn Sayyaadi. "Simple-II: a new numerical thermal model for predicting thermal performance of Stirling engines." *Energy* 69 (2014): 873-890. <https://doi.org/10.1016/j.energy.2014.03.084>
- [42] Li, Ruijie, Lavinia Grosu, and Diogo Queiros-Condé. "Losses effect on the performance of a Gamma type Stirling engine." *Energy Conversion and Management* 114 (2016): 28-37. <https://doi.org/10.1016/j.enconman.2016.02.007>
- [43] Mabrouk, Mohamed Tahar, Abdelhamid Kheiri, and Michel Feidt. "Effect of leakage losses on the performance of a β type Stirling engine." *Energy* 88 (2015): 111-117. <https://doi.org/10.1016/j.energy.2015.05.075>
- [44] Moran, Michael J., Howard N. Shapiro, Daisie D. Boettner, and Margaret B. Bailey. *Fundamentals of engineering thermodynamics*. John Wiley & Sons, 2014.
- [45] El-Ghafour, S. "Design and Computational Fluid Dynamics Simulation of a Solar Stirling Engine." PhD diss., Ph. D. Dissertation, University of Port Said, Port Said, Egypt, 2018.
- [46] Colpan, C. Ozgur, and Tülay Yeşin. "Energetic, exergetic and thermoeconomic analysis of Bilkent combined cycle cogeneration plant." *International Journal of Energy Research* 30, no. 11 (2006): 875-894. <https://doi.org/10.1002/er.1192>
- [47] Ergun, Sabri, and Ao Ao Orning. "Fluid flow through randomly packed columns and fluidized beds." *Industrial & Engineering Chemistry* 41, no. 6 (1949): 1179-1184. <https://doi.org/10.1021/ie50474a011>
- [48] Walker, G., and V. Vasishta. "Heat-transfer and flow-friction characteristics of dense-mesh wire-screen Stirling-cycle regenerators." In *Advances in Cryogenic Engineering*, pp. 324-332. Springer, Boston, MA, 1971. https://doi.org/10.1007/978-1-4757-0244-6_41
- [49] Thieme, Lanny G. "High-power baseline and motoring test results for the GPU-3 Stirling engine." (1981).
- [50] Costa, S. C., Harritz Barrutia, Jon Ander Esnaola, and Mustafa Tutar. "Numerical study of the pressure drop phenomena in wound woven wire matrix of a Stirling regenerator." *Energy Conversion and Management* 67 (2013): 57-65. <https://doi.org/10.1016/j.enconman.2012.10.014>

-
- [51] Tlili, I., Y. Timoumi, and S. Ben Nasrallah. "Numerical simulation and losses analysis in a Stirling engine." *Int. J. Heat Technol* 24, no. 1 (2006): 97-105.